



Macroanatomy and 3D probabilistic atlas of the human insula

Isabelle Faillenot, Rolf Heckemann, Maud Frot, Alexander Hammers

► To cite this version:

Isabelle Faillenot, Rolf Heckemann, Maud Frot, Alexander Hammers. Macroanatomy and 3D probabilistic atlas of the human insula. *NeuroImage*, 2017, 150, pp.88-98. 10.1016/j.neuroimage.2017.01.073 . inserm-03551069

HAL Id: inserm-03551069

<https://inserm.hal.science/inserm-03551069>

Submitted on 1 Feb 2022

HAL is a multi-disciplinary open access archive for the deposit and dissemination of scientific research documents, whether they are published or not. The documents may come from teaching and research institutions in France or abroad, or from public or private research centers.

L'archive ouverte pluridisciplinaire **HAL**, est destinée au dépôt et à la diffusion de documents scientifiques de niveau recherche, publiés ou non, émanant des établissements d'enseignement et de recherche français ou étrangers, des laboratoires publics ou privés.



Macroanatomy and 3D probabilistic atlas of the human insula

Isabelle Faillenot^{a,b}, Rolf A. Heckemann^{c,d,e}, Maud Frot^{b,f}, Alexander Hammers^{c,g,*}

^a Neurology Department – Hôpital Nord, 42055 Saint-Etienne, France

^b Central Integration of Pain Unit – Lyon Center for Neuroscience (CRNL), INSERM1028, 69675 Lyon, France

^c Neurodis Foundation, 69675 Lyon, France

^d MedTech West at Sahlgrenska University Hospital, University of Gothenburg, Sweden

^e Division of Brain Science, Imperial College London, UK

^f Claude Bernard University Lyon 1, Villeurbanne 69000, France

^g King's College London & Guy's and St Thomas' PET Centre, King's College London, Division of Imaging Sciences and Biomedical Engineering, London, UK

ARTICLE INFO

Keywords:

Neuroanatomy
Insula anatomy
Computer-assisted image processing
Magnetic resonance imaging methods
Statistics and numerical data
Neurological models
Sex characteristics

ABSTRACT

The human insula is implicated in numerous functions. More and more neuroimaging studies focus on this region, however no atlas offers a complete subdivision of the insula in a reference space. The aims of this study were to define a protocol to subdivide insula, to create probability maps in the MNI152 stereotaxic space, and to provide normative reference volume measurements for these subdivisions.

Six regions were manually delineated bilaterally on 3D T1 MR images of 30 healthy subjects: the three short gyri, the anterior inferior cortex, and the two long gyri.

The volume of the insular grey matter was $7.7 \pm 0.9 \text{ cm}^3$ in native space and $9.9 \pm 0.6 \text{ cm}^3$ in MNI152 space. These volumes expressed as a percentage of the ipsilateral grey matter volume were minimally larger in women ($2.7 \pm 0.2\%$) than in men ($2.6 \pm 0.2\%$). After spatial normalization, a stereotactic probabilistic atlas of each subregion was produced, as well as a maximum-probability atlas taking into account surrounding structures.

Automatically labelling insular subregions via a multi-atlas propagation and label fusion strategy (MAPER) in a leave-one-out experiment showed high spatial overlaps of such automatically defined insular subregions with the manually derived ones (mean Jaccard index 0.65, corresponding to a mean Dice index of 0.79), with an average mean volume error of 2.6%.

Probabilistic and maximum probability atlases and the original delineations are available on the web under free academic licences.

1. Introduction

The human insula is implicated in pain perception, autonomic control, emotion processing, and numerous other functions (for a review see Nieuwenhuys, 2012) as shown by clinicopathological correlations (Ibañez et al., 2010; Jones et al., 2010), exploration with intracranial depth electrodes (Ostrowsky et al., 2002; Peyron et al., 2004), and functional neuroimaging (Garcia-Larrea, 2012; Nieuwenhuys, 2012; Craig et al., 2000; Peyron et al. 2013). Functional activities in the insula were historically roughly localized relatively to the anterior or posterior insula lobule separated by the central sulcus. More accurate spatial localization can be achieved by reference to macroanatomical subdivisions.

1.1. Subdivisions

Previous work identified at least five main insular gyri with a radial orientation towards the ventral pole (Affif et al., 2013; Naidich et al., 2004). Little is known on how functions are topographically organized in the insular cortex, and studies have revealed incomplete correspondence between gyral organization and functional organization (Cauda et al., 2011; Craig, 2009; Deen et al., 2011; Kurth et al., 2010b). However, interlaboratory comparisons are usually based on macro-anatomical landmarks: 1) MNI (or, largely historically, Talairach coordinates) are defined after spatial deformations of individual brains based on overall morphology; 2) these landmarks are often the only reference available to localize functional results. No available atlas

* Correspondence to: King's College London & Guy's and St Thomas' PET Centre, Division of Imaging Sciences and Biomedical Engineering, King's College London, 4th floor Lambeth Wing, St Thomas' Hospital, Westminster Bridge Road, London SE1 7EH, UK.

E-mail address: alexander.hammers@kcl.ac.uk (A. Hammers).

<http://dx.doi.org/10.1016/j.neuroimage.2017.01.073>

Received 6 December 2015; Received in revised form 16 December 2016; Accepted 30 January 2017

Available online 04 February 2017

1053-8119/© 2017 The Authors. Published by Elsevier Inc. This is an open access article under the CC BY license (<http://creativecommons.org/licenses/by/4.0/>).

offers a complete subdivision and accurate statistical description of the gyral insular organization.

Cytoarchitecture can serve as a putative anatomical substrate of functional organization. Insular architectonic maps suggest a near concentric organization almost perpendicular to the gyral organization (Mesulam and Mufson, 1985; Bonthuis et al., 2005; Morel et al., 2013). The insula is divided into a dorsocaudal granular zone and an agranular rostroventral region (Brodmann, 1909). The additional delineation of an intermediate dysgranular part, as well as the exact location of the borders between these regions, varies widely between maps. Moreover, some studies indicated that the microanatomy is more complicated than a simple concentric pattern (Brockhaus, 1940; Rose, 1928). Cytoarchitectonic maps, elaborated on ex-vivo data from small samples of subjects, are difficult to use in neuroimaging studies for several reasons: 1) they are not generally accessible from *in vivo* data, 2) they are difficult to align with the 3D data from neuroimaging experiments, and 3) they do not generally account for intersubject variability. It is noteworthy that the 3D probabilistic cytoarchitectonic maps contained in the Anatomy Toolbox (Eickhoff et al., 2005) take into account these important limitations. However, these maps include three areas in the posterior part of the insular cortex only (Ig1, Ig2 and Id1) (Kurth et al., 2010a).

Atlases can be deterministic or probabilistic. Deterministic atlases define fixed boundaries and do not directly account for interindividual variability. A probabilistic atlas is created by segmenting multiple subjects' brains, spatially normalizing them to match a template, and then consolidating the normalized segmentations. Two types of maps can be created, which both consider the interindividual variability present in the data. In a probabilistic map, the value of each voxel indicates the probability that this location corresponds to a specific anatomical structure. In a maximum probability map, each voxel is labeled according to the anatomical structure to which it most likely belongs (Hammers et al., 2003). Finally, multiple individual atlases can be used in multi-atlas registration and label propagation schemes (e.g. Heckemann et al. 2006; MAPER – Heckemann et al. 2010). Such strategies achieve labelling accuracies that approach those of human observers (Hammers et al., 2007a, 2007b) (Fig. 1).

1.2. Morphology

The macroanatomical delineation of the insula was described by Türe et al. (1999) and Naidich et al. (2004). The insular central sulcus (CS) is the main sulcus that divides the insula obliquely into anterior and posterior lobules. It runs from posterior superior to anterior inferior. Anteriorly, the precentral sulcus (preCS) separates the posterior short gyrus (PSG) from the middle short gyrus (MSG); the short insular sulcus (SIS) separates the MSG from the anterior short gyrus (ASG). An accessory gyrus (AG) was described anterior to the ASG, often confined to the anterior surface. The transverse gyrus (TG) joins the inferior portion of the anterior insula with the posterior orbito-frontal region. The anteroinferior part of the insula includes the apex where the short gyri converge (also called insular operculum by some authors) and the limen insulae. Posterior to the CS, the postcentral sulcus (postCS) separates the anterior long gyrus (ALG) and the posterior long gyrus (PLG).

These authors also described the relationships of insular gyri with overlying opercula. The anterior insula is connected with the frontal lobe and the posterior insula with both the parietal and temporal lobes. The three more anterior gyri (AG, TG and ASG) are continuous with the orbital gyri. The IFG (pars opercularis) covers the ASG and MSG. The inferior part of the postcentral gyrus is over the PSG and the superior part of ALG and PLG. The inferior part of the posterior lobule is adjacent to the Heschl gyrus and is covered by temporal operculum. These descriptions were used to define the protocol to subdivide the insulae in our study, which has allowed us to provide a quantification of how frequently different anatomic features were found in the insulae of the 30 subjects.

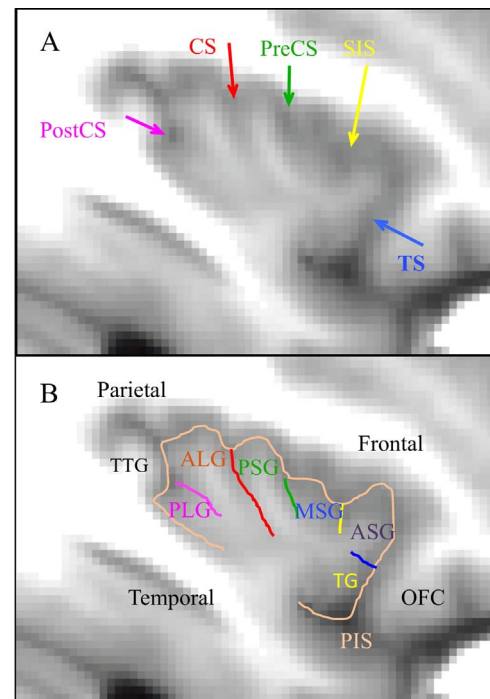


Fig. 1. Main structures drawn on left insula of the average MRI of 30 subjects. A: main insular sulci pointed by arrows. CS: central; PostCS: postcentral; PreCS: precentral; SIS: short insular; TS: transverse. B: Drawing of sulci and labeling of gyri. ALG: Anterior long; ASG: Anterior short; TTT: transverse temporal; MSG: middle short; OFC: orbito-frontal cortex; PIS: peri-insular sulcus; PLG: posterior long; PSG: posterior short; TG: transverse.

1.3. Volumes

Gender effects may be important because the insula in males, like numerous other cerebral regions, is larger than in females (eg Afif et al., 2009). The volume of the insula relative to the total grey matter (GM) volume has not been documented, although it is estimated that the surface of the insulae takes 1.8% of the total cortical surface area (Tramo et al., 1995) and the insular volume is 1.4% of the total hemisphere volume (white matter included, Semendeferi and Damasio, 2000).

The typical amount of right/left asymmetry of the insular volume is debated: some papers report no asymmetry (Afif et al., 2009; Hammers et al., 2003), while others show leftward asymmetry (Cunningham, 1891; Hervé et al., 2006). Keller et al. (2010) suggested that there is a subtle but significant positive correlation between the extent of hemispheric language dominance and insula volume asymmetry, indicating that a larger insula predicted functional lateralization to the same hemispheric side for the majority of subjects.

1.4. Objectives

The aims of this study were to create protocols for macroscopically subdividing the insula in native space. These then served to provide typical structure volumes and spatial extents in native and stereotaxic space in healthy adults; to define a normal range; and to look for asymmetry (R/L comparison) and gender effects.

The delineations were additionally used to construct probabilistic atlases of insular gyri in MNI152 stereotaxic space. Morphological features of the thirty right and thirty left insulae were investigated.

We also built a deterministic maximum probability map for easy use with standard software packages. Finally, individual segmentations and their associated anonymized MRIs were used in multi-atlas label propagation software to assess the accuracy of automated anatomical segmentations of individual subjects' MRIs enabled by the new atlases.

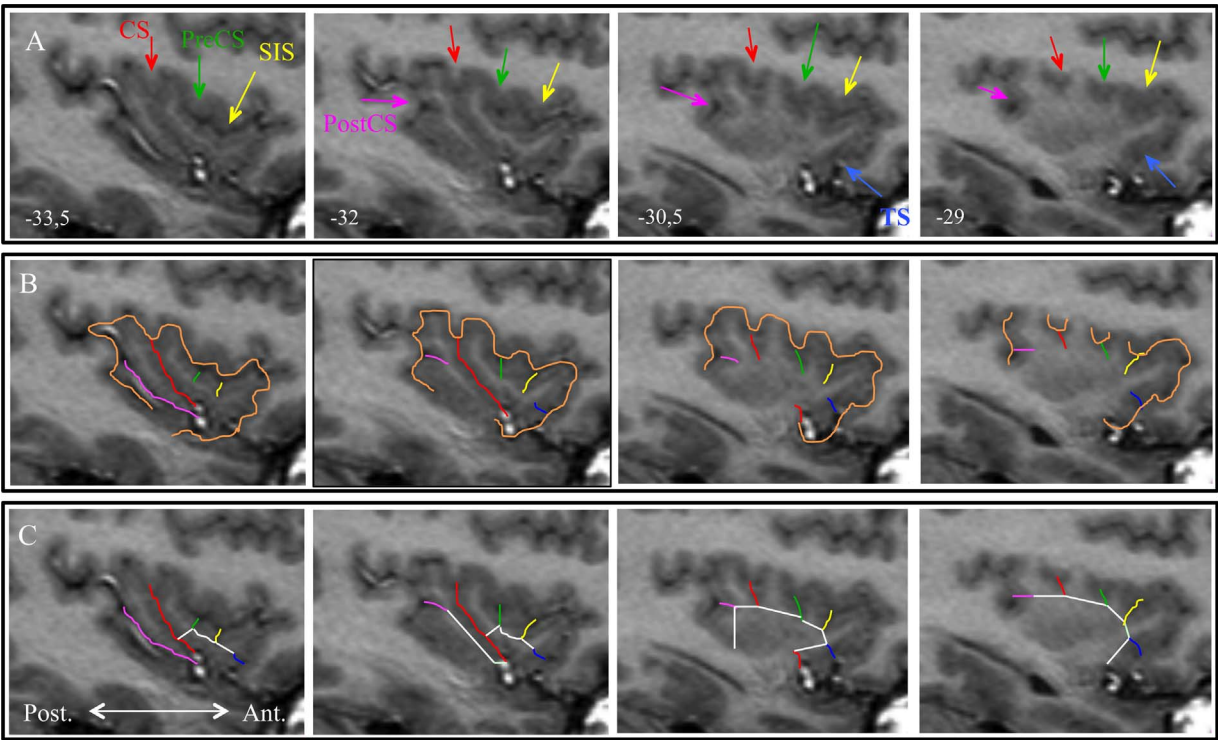


Fig. 2. Illustration of insula borders as they were defined in the protocol. Left insula of subject 9 (A9L). Numbers indicate the distance (mm) from midsagittal plane. A. Location of the sulci on sagittal slices. Red = central sulcus; green = precentral sulcus; yellow = short insular sulcus; blue = transverse sulcus; pink = postcentral sulcus; orange = peri-insular sulcus. B. Drawing of the sulci that were used to separate the insular regions. C. Borders which are not defined by sulci (in white).

2. Methods

Six subregions of the adult insula were delineated on the magnetic resonance (MR) images used in the construction of the “Hammers_mith” brain atlases described in [Hammers et al. \(2003, 2007a\)](#) and [Gousias et al. \(2008\)](#), which are available at www.brain-development.org. At study start, these atlases consisted of 83 entirely manually delineated regions drawn on MR images of 30 healthy subjects in native space. Subjects had no neurological, medical, or psychiatric conditions and had normal MR scans. The cohort consisted of 15 women (median age: 31 years; range: 20–54) and 15 men (median age: 30 years; range: 20–53), and 25 of the 30 subjects were right-handed. In these atlases, the insula was defined as a single region following the protocol in ([Hammers et al. 2003](#)).

2.1. Nomenclature

We followed the English nomenclature used by [Türe et al. \(1999\)](#). [Fig. 2](#) shows a sample of macro-anatomical landmarks, and [Table 1](#) lists the abbreviations used in this paper. Our definition departs from [Türe et al. \(1999\)](#) and [Naidich et al. \(2004\)](#) with regard to the two less stable gyri: AG and TG. They described AG in front of the ASG, often confined to the anterior surface. Since they did not describe a clear separation from the ASG, we decided to include the AG (when present) in the anteriormost region (ASG). The TG joins the inferior portion of the anterior insula with the posterior orbitofrontal region. The sulcus that defines the superior border of the TG has not been described elsewhere to our knowledge; we will refer to it as the transverse sulcus (TS). The term anterior inferior cortex (AIC) is used here to identify the anteroinferior part of the insula including the apex, the limen and the transverse gyrus.

2.2. Protocol definition

The exterior edge of the insula had been defined in [Hammers et al.](#)

Table 1
Abbreviations.

Abbreviation	Name
AG	Accessory gyrus
ALG	Anterior long gyrus
ASG	Anterior short gyrus
CS	Central sulcus
GM	Grey matter
IFG	Inferior frontal gyrus
AIC	Anterior inferior cortex (apex+limen+pole+TG)
IPL	Inferior parietal lobule
MSG	Middle short gyrus
PIS	Peri-insular sulcus
PLG	Posterior long gyrus
postCG	Postcentral (parietal) gyrus
postCS	Postcentral (insular) sulcus
preCG	Precentral (frontal) gyrus
preCS	Precentral (insular) sulcus
PSG	Posterior short gyrus
SIS	Short insular sulcus
STG	Superior temporal gyrus
TG	Transverse (insular) gyrus
TS	Transverse sulcus

(2003), using the peri-insular sulcus as the main border. We noticed that there was a frequent error in the previous atlas: the posterior boundary was often set to the posterior ascending ramus of the Sylvian fissure instead of the inferior PIS. In these cases, we corrected the posterior border of the insula as the anterior border of the transverse temporal gyrus, which had previously been included in the superior temporal gyrus (STG) of the atlas (see [Fig. 2B](#)). The voxels located in this region were reassigned and the definition of the STG (see [Hammers et al., 2003](#)) was changed accordingly. The STG region now includes: 1) the transverse temporal gyrus even if it extends posteriorly of the last coronal slice where hippocampus is measured; 2) cortex located posteriorly to the transverse temporal gyrus in the planum temporale. Occasionally, very few voxels, previously labeled

insula, were included in the supramarginal gyrus when located in the parietal operculum. More importantly, remaining voxels located in this region were in the white matter and were no longer defined by the protocols of insula and STG, so they were labeled “background”, i.e. not classified as any region, usually contiguous with the internal capsule or optic radiation which do not have a separate label.

2.3. Manual segmentation and normalization to MNI152 space

We used Rview v9 (<http://rview.colin-studholme.net/>) to segment the images in their native space. Morphological characteristics of the insula were assessed on three orthogonal views of the MR image and simultaneously on its surface rendering. Segmentations were performed in the sagittal plane and confirmed in other planes as well as on the surface rendering of the insula. The prior segmentations (Hammers et al., 2003, Gousias et al., 2008) were visible during this new segmentation. The rater carrying out the delineations was blinded to subject information such as gender and age.

The anatomical segmentation of the insulae yielded 30 separate atlases in native space, where each subregion was identified by a unique voxel value.

The T1-weighted MR volume of each subject was spatially normalized to a widely used T1-weighted MR image template in stereotaxic space, the Montreal Neurological Institute/International Consortium for Brain Mapping (MNI/ICBM) as contained in the Statistical Parametric Mapping (SPM8) package (Wellcome Department of Imaging Neuroscience, available at <http://www.fil.ion.ucl.ac.uk/spm>). We used the iterative “unified segmentation” procedure implemented in SPM8 (Ashburner and Friston, 2005) that yielded probabilistic maps of grey and white matter and other tissues as well as the transformation from native to MNI152 space. The warping parameters thus determined from the MR images were then applied to the complete atlases that were in the same space as the native MR volume. We used nearest-neighbour interpolation to preserve allocation of a given voxel to a unique region. The grey matter (GM) image was thresholded to generate a mask of voxels having at least 50% probability of being gray matter. This GM mask was also normalized with the same parameters. The spatially normalized images were resampled with isotropic voxel sizes of $1.5 \times 1.5 \times 1.5 \text{ mm}^3$ in a matrix of x/y/z dimensions of 121/145/121 voxels. The normalized MR images were averaged across subjects to yield an image representing the group for illustration purposes.

2.4. Multi-atlas label propagation

To estimate the accuracy with which the subregion labels can be transferred from the atlas database to newly acquired images, we carried out multi-atlas label propagation segmentations in a standard leave-one-out cross-comparison using MAPER software (Heckemann et al., 2010). Each of the atlas MR images was treated as the segmentation target in turn, using the remaining 29 atlases as label sources. The automatically generated insular subregion labels were assessed by comparison with the target subject's manual labels, using the Jaccard index (intersection divided by union) to quantify label overlap (Jaccard, 1901) and the volume error to quantify volumetric aberration.

2.5. Data collection and statistics

Morphological information was collected for each insula. Presence or absence was noted of each sulcus and gyrus and the opercular regions (as defined in Hammers et al., 2003 and Gousias et al., 2008) which are in contact with each insular gyrus.

Using FSL (FMRIB Software Library, Jenkinson et al., 2012), native and normalized atlases were masked with their corresponding thresholded GM image. For each subregion, a probabilistic map was

created by adding the normalized GM-masked atlases across subjects. Each increment in voxel intensity corresponds to an increase of the probability of encountering the given subregion at this location of $1/30 \approx 3.3\%$. The maximum probability map was created by combining all region definitions using vote-rule fusion. Each voxel is labelled according to the anatomical structure to which it most likely belongs.

The volumes of each insular region as well as the total insula volume were sampled from the GM-masked atlases in native and normalized space. As volumes are influenced by the overall brain size (Bauernfeind et al., 2013), insula volumes were also expressed as a percentage of ipsilateral GM volume, and sub-insular regions were expressed as a percentage of ipsilateral insular volume. For comparability with previous studies, the volume of each insula was also expressed as a percentage of the intracranial volume (ICV), which was calculated as described in Lemieux et al. (2003).

To estimate the variability of each subregion, we calculated the percentage of voxels assigned to the same region in all subjects (thus having a probability of 100%).

The influence of gender, side and age on insula volumes in native space was assessed using ANOVA with volume as dependent variable; gender and laterality as fixed factors and age as covariable. The comparisons were done for absolute volumes, volumes relative to ipsilateral GM volume and volume relative to ICV.

3. Results

3.1. Protocols for subdivisions

The delineation of each insula proceeded in two steps. First, borders were traced in order to assign a region for all the GM voxels (Fig. 2). This was done on sagittal slices in antero-posterior order, as listed below. White matter inside these edges was included in the region. Second, remaining unassigned insular white matter was assigned to each subdivision.

3.1.1. Anterior short gyrus (ASG): labels 86 (left) and 87 (right)

This region includes the accessory gyrus if present.

Posterior border: short insular sulcus (SIS)

Inferior border: line from the deepest point of SIS to the deepest point of transverse sulcus (TS).

Other borders: external border of insula.

NB: If the TS is absent or unclear (e.g. Fig. 3 A1L; Supplementary Figure 1) or if there are two sulci (e.g. Fig. 3 A4L, Supplementary Figure 2), then defining the inferior boundary is underpinned by these general principles: 1) the posterior orbital gyrus often bends into the insula and the point of the steepest curve is often in front of the TS; 2) the TS is often between the middle and the inferior third of the anterior insular border on sagittal slices; 3) the AIC is often close to the posterior orbital gyrus; 4) the TG is a horizontal gyrus whereas AG and ASG are generally vertical gyri.

3.1.2. Middle short gyrus (MSG): labels 88 (left) and 89 (right)

Anterior border: short insular sulcus (SIS)

Posterior border: precentral sulcus (PreCS)

Inferior border: line from the deepest point of PreCS to the deepest point of SIS

Other borders: external border of insula.

NB:

1. If the MSG according to this definition is absent (e.g. Fig. 3 A1L, Supplementary Figure 3), a protrusion on the neighboring gyri was labeled MSG.

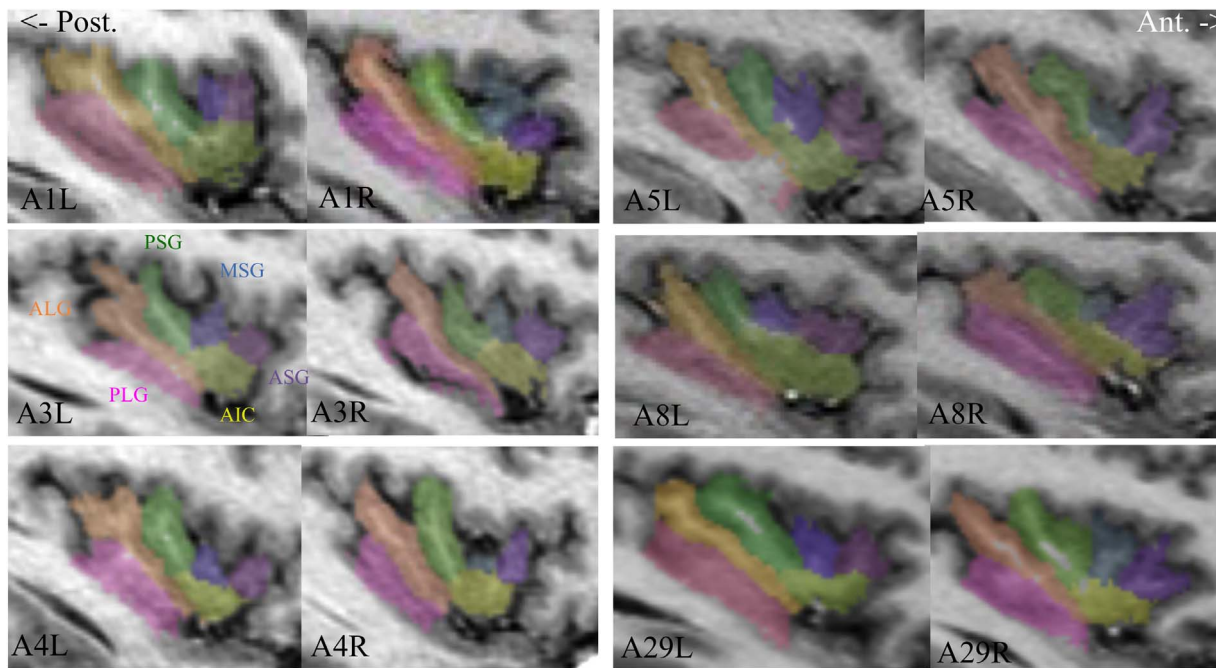


Fig. 3. Examples of segmented insulae of six subjects showing variability of insular anatomy. Legends indicate subject number and side (L/R). Pink: Posterior long gyrus (PLG); orange: anterior long gyrus (ALG); green: posterior short gyrus (PSG); blue: middle short gyrus (MSG); purple: anterior short gyrus (ASG); yellow: anterior inferior cortex (AIC). A1L has no separate MSG, but a protrusion on the ASG was labelled as MSG. A1L & A3L do not have a clear boundary between ASG and AIC. A4R & A29L have a long pre-central sulcus that reaches the peri-insular sulcus. A5LR & A8R & A29R have a prominent accessory gyrus, which can also be seen as a bifid ASG. A8R shows a discontinuous central sulcus.

2. If there are more than two sulci in the anterior insula (for example in the case of bilobar gyri, e.g. Fig. 3 A5L, Supplementary Figure 4), the preCS is generally almost parallel to the central sulcus.
3. If the preCS traverses the insula to the inferior PIS (e.g. Fig. 3 A29L, Supplementary Figure 5), the inferior border is a line drawn perpendicular to the preCS from the end of the SIS.

3.1.3. Posterior short gyrus (PSG): labels 90 (left) and 91 (right)

Anterior border: precentral sulcus (PreCS)

Posterior border: central sulcus (CS)

Inferior border: A line from the deepest point of the CS to the deepest point of the PreCS. When the CS extends to the PIS, this border is a line drawn perpendicular to the central sulcus from the end of the PreCS.

Other borders: external border of insula.

NB: If the preCS also traverses the insula up to the inferior PIS (e.g. Fig. 3 A29L, Supplementary Figure 5), then instead of the deepest point of the preCS, the intersection point between the preCS and the inferior border of MSG is used.

3.1.4. Anterior inferior cortex (AIC): labels 92 (left) and 93 (right)

It includes the apex, the limen and the transverse gyrus (if present).

Superior border: inferior borders of ASG, MSG and PSG. On slices where the CS is discontinuous, trace the boundary between end of TS and end of inferior part of CS through WM (use a curve in order not to cut gray matter)

Posterior border: central sulcus (CS)

Other borders: external border of insula

3.1.5. Anterior long gyrus (ALG): labels 94 (left) and 95 (right)

Anterior border: central sulcus (CS)

Inferior border: postcentral sulcus (postCS) or a line from deepest point of CS to deepest point of postCS.

Other borders: external border of insula

NB: Since Naidich et al. (2004) observed that the ALG could be bifid and that the PLG is never split in two, when two sulci were present in the posterior lobule we considered ALG bifid (e.g. Fig. 3 A3L).

3.1.6. Posterior long gyrus (PLG): labels 20 (left) and 21 (right)

All remaining insular grey matter postero-inferiorly to the ALG.

3.1.7. White matter assignment

Remaining unassigned insular white matter was assigned to each subdivision: on coronal slices, a horizontal line was traced from the subdivision boundary until a more medial structure was reached.

3.2. Probabilistic maps

Probabilistic maps of each subregion are displayed on sagittal sections across the left and right insulae (Fig. 4), where white voxels denote a probability of 100% of the subregion being present in that voxel in MNI152 space, and black ones a probability of 6.7% (two subjects). Fig. 5 represents these maps thresholded at 50%; see also the supplementary Fig. 9–11 for a representation in the three orthogonal planes.

Another means of representing variability across subjects is to sum the borders of each ROI after MNI normalization (see Fig. 12 in the Supplementary Material).

The location of the PLG is the most consistent, with 14% (262 mm³) of the mean volume with a probability of 100% (Table 2). The MSG is the least consistent with only 0.7% of the mean volume (7 mm³) common to all 30 subjects.

The spatially normalized delineations were integrated into the Hammersmith n30r83 maximum probability atlas which, together with the newly added angular and supramarginal gyri (Wild et al., submitted), yields the Hammersmith n30r95 maximum probability atlas.

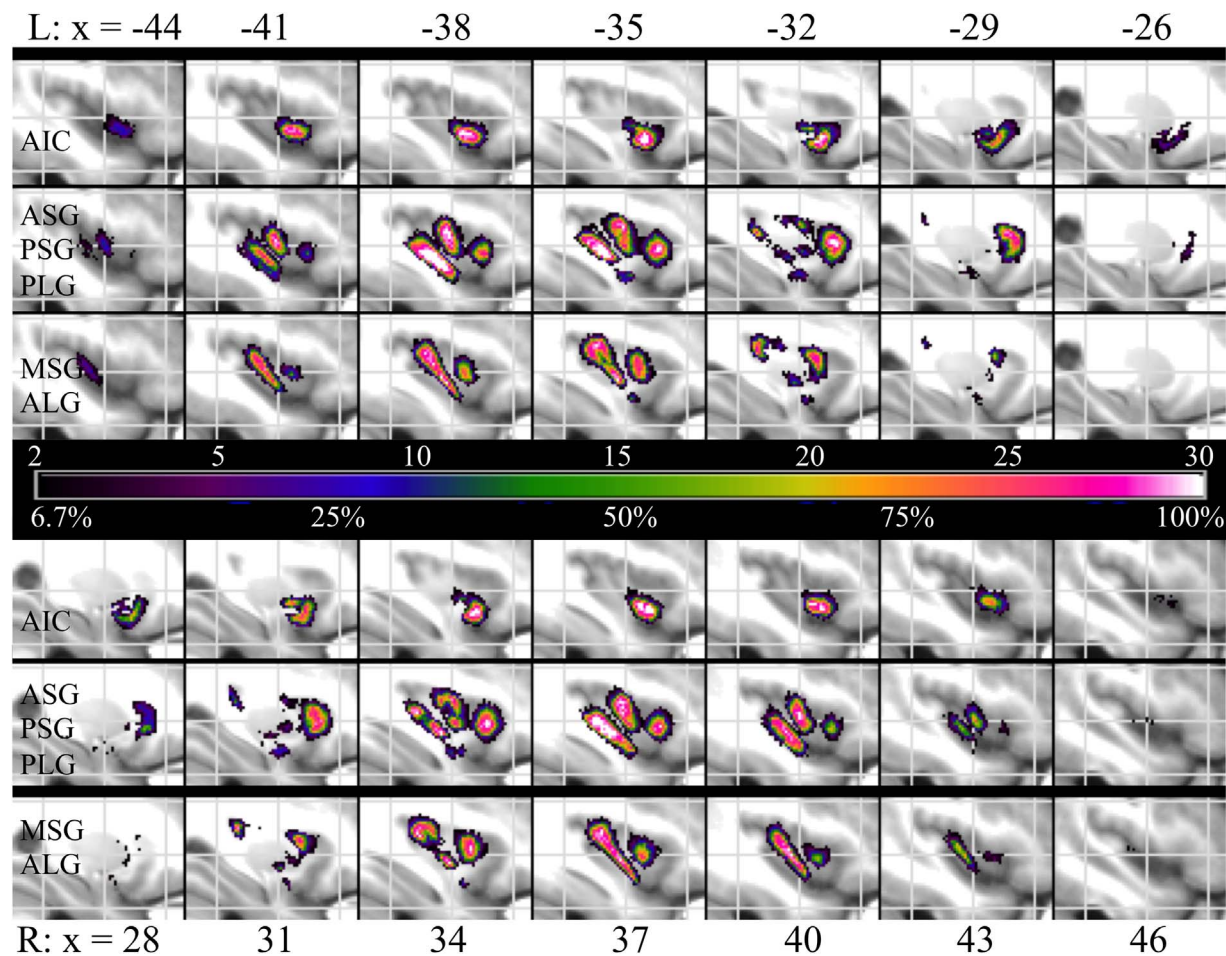


Fig. 4. Probabilistic maps of subregions of left (L) and right (R) insula superimposed on the average of the 30 MR images in MNI152 space. Colors represent the prevalence of the various subregions at this location in number of subjects, as well as the probability of encountering the subregion as a percentage. Lines 1 and 4 represent the AIC; lines 2 and 5 represent ASG, PSG and PLG; lines 3 and 6 represent MSG and ALG. Gray lines indicate planes: $y=0$, $z=0$, $y= \pm 35\text{mm}$ and $z= \pm 30\text{ mm}$. x indicate the sagittal plane (mm from midsagittal plane).

3.3. Morphology

The examples cited below refer to Fig. 3, which shows samples of subdivided insulae of six subjects. The CS was always present and crossed the insula obliquely to reach the falciform fold. It was discontinuous only once among the 30 right and 30 left insulae (A8R). The PreCS crossed the insula up to the inferior PIS in 48% (e.g. A4R, A29L). The PostCS was long and defined a well-formed PLG in 55% (e.g. A8R). The TS was well seen in 57% (e.g. A1R, A3R, A4R).

Table 3 indicates the structures found in the 30 right and 30 left insulae, including those not individualized by the final protocol. ASG, PSG, AIC, ALG and PLG were always present. The AG was present in

Table 2
Volume of the common portion in all subjects for each subregion (white voxels of the probability maps). mm^3 : mean volume of the 100% probability shell. %: percentage of the common volume vs mean MNI volume of that subregion.

Volumes	mm^3	%
ASG	47	3.0
MSG	7	0.7
PSG	61	4.0
AIC	132	6.7
ALG	56	2.8
PLG	262	14.0

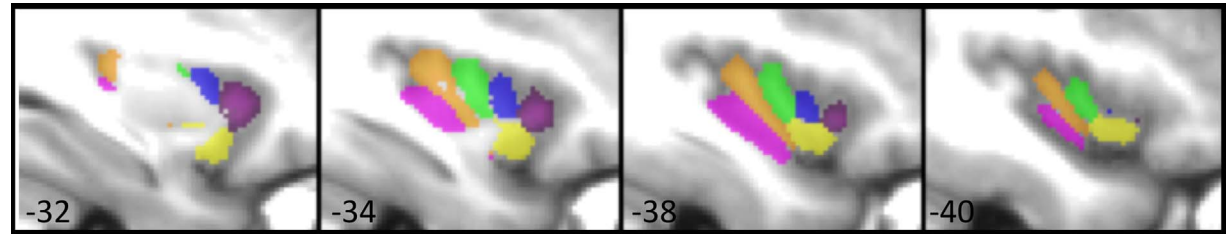


Fig. 5. Left insular subdivisions of the probabilistic maps thresholded at 50% superimposed on the average of the 30 MRIs. Pink: Posterior long gyrus (PLG); orange: anterior long gyrus (ALG); green: posterior short gyrus (PSG); blue: middle short gyrus (MSG); purple: anterior short gyrus (ASG); yellow: anterior inferior cortex (AIC).

Table 3

Presence of the various subdivisions in the 30 right and 30 left insulae (in percent), and their repartition in the left and right sides and in the male and female subjects.

Region	Present (%)	Laterality (L/R)	Gender (M/F)
ASG	100	30 / 30	30/30
MSG	95	29 / 28	29/28
PSG	100	30 / 30	30/30
AIC	100	30 / 30	30/30
ALG	100	30 / 30	30/30
PLG	100	30 / 30	30/30
AG	50	15 / 15	17/13
TG	57	14 / 20	21/13
Posterior pole	40	9 / 15	14/10

50% of the insulae (18% were prominent, e.g. A5L). The TG is often difficult to distinguish from the pole itself. It was clearly distinct from the pole in 57% of cases (e.g. A8L). The MSG was absent in 5% (e.g. A1L) and the MSG label was then applied as described in the protocol. A posterior pole was easy to distinguish in only 40% of insulae (e.g. A4L, A5L). Of the few small differences between hemispheres and men and women in terms of presence of structures, only the presence of a TG was borderline significantly more common in males (chi-square test, $p < 0.04$, uncorrected for multiple comparisons).

Table 4 indicates, for each insular subregion, the adjacent opercular cortex. The ASG was covered by the inferior frontal gyrus alone in all cases. The MSG was covered in 90% of cases by IFG. The PSG was covered by the PreCG in 93% of all insulae. The AIC was always covered by the anterior superior temporal gyrus (anterior to the amygdalar coronal planes). The superior part of ALG was hidden by PostCG in 98% of cases and its inferior part was always covered by the superior temporal gyrus (posterior part). The whole PLG was covered by the posterior STG in all cases.

Table 4

Percentage of the 60 insulae (number in left and right hemisphere) with adjacency between an insular subregion and a particular opercular region. Except for ASG and PLG, insular subregions were in contact with more than one opercular region.

Insular subdivision	Opercular cortex	ASG	MSG	PSG	AIC	ALG	PLG
IFG		100 (30 / 30)	90 (27 / 27)	35 (7 / 14)	72 (23 / 20)	0	0
PreCG		0	47 (19 / 9)	93 (27 / 29)	27 (8 / 8)	23 (6 / 8)	0
PostCG		0	0	62 (19 / 18)	0	98 (28 / 30)	0
IPL		0	0	0	0	42 (10 / 15)	0
anterior STG		0	0	0	100 (30 / 30)	0	0
posterior STG		0	0	0	28 (10 / 7)	100 (30 / 30)	100 (30 / 30)

Table 5

Volume averaged across the 60 (right + left) grey matter portions of the insulae (mm^3) and their relative part in the total GM volume (% volume). SD: standard deviation. CV: coefficient of variation (SD/Mean). % volume: volume of insular subregions is expressed as a percentage of ipsilateral insular volume; volume of insula is expressed as a percentage of the volume of the ipsilateral hemisphere. Insula M/F: mean insular volume of the 15 males or 15 females. Insula L/R: volume of the 30 left or 30 right insulae.

	Volume \pm SD (CV)		% volume \pm SD (CV)	
	Native	MNI152	Native	MNI152
ASG	1238 \pm 270 (22%)	1589 \pm 241 (15%)	16.1 \pm 3.1 (20%)	16.0 \pm 2.4 (15%)
MSG	750 \pm 221 (29%)	966 \pm 173 (18%)	9.7 \pm 2.6 (26%)	9.7 \pm 1.7 (17%)
PSG	1141 \pm 265 (23%)	1487 \pm 273 (18%)	14.9 \pm 3.3 (22%)	15.0 \pm 2.7 (18%)
AIC	1578 \pm 431 (27%)	1979 \pm 408 (21%)	20.3 \pm 4.5 (23%)	19.9 \pm 3.6 (18%)
ALG	1573 \pm 251 (16%)	2020 \pm 242 (12%)	20.5 \pm 2.9 (14%)	20.4 \pm 2.3 (11%)
PLG	1443 \pm 282 (20%)	1876 \pm 230 (12%)	18.7 \pm 2.5 (13%)	18.9 \pm 1.8 (10%)
Insula M	8025 \pm 1006 (13%)	9740 \pm 536 (5%)	2.60 \pm 0.19 (7%)	2.63 \pm 0.11 (4%)
Insula F	7415 \pm 693 (9%)	10122 \pm 639 (6%)	2.74 \pm 0.23 (8%)	2.69 \pm 0.19 (7%)
Insula L	7721 \pm 872 (11%)	9944 \pm 633 (6%)	2.68 \pm 0.21 (8%)	2.67 \pm 0.15 (6%)
Insula R	7725 \pm 964 (12%)	9887 \pm 705 (7%)	2.67 \pm 0.23 (9%)	2.64 \pm 0.17 (6%)
Insula	7723 \pm 912 (12%)	9915 \pm 610 (6%)	2.67 \pm 0.22 (8%)	2.66 \pm 0.16 (6%)

3.4. Volumes

Native and normalized volumes of the whole insula and of each subregion are shown in Table 5. ANOVA showed that there was an effect of gender (but no effect of age or side) on absolute and on relative insular GM volumes ($p = 0.010$ and 0.015 respectively). While the absolute insular volume is larger in men than in women, the insular volume represents a larger fraction of the GM volume in women ($2.74 \pm 0.23\%$) than in men ($2.60 \pm 0.19\%$). ANOVA with volumes relative to the ICV showed the same results: the insular grey matter had a volume representing $0.62 \pm 0.06\%$ of ICV in men, whereas it occupied $0.66 \pm 0.06\%$ in women. This was also true after normalization to MNI space (Table 5 Column 3), which represents another normalization for global volume (Hammers et al., 2003).

3.5. Multi-atlas propagation of insular subregion labels

There was strong agreement between subregion labels generated with MAPER and those that had been delineated manually (Table 6). The overlap results (mean Jaccard index 0.65, corresponding to a Dice index of 0.79) are in line with those we previously found for regions of comparable size and shape (Heckemann et al. 2010). The average mean volume error was 2.6%.

4. Discussion

We present the first statistical multi-subject atlas database of the macroscopical anatomy of the human insula. This work provides normative macroanatomical reference data for localizing functional activation and for assessing structural change in the wake of pathological processes. In addition, the ensemble of atlases and their associated MR images can be used for accurate multi-atlas automatic segmentation of individual target images (e.g. MAPER; Heckemann et al., 2010).

Table 6

Results of the multi-atlas label propagation for each sub-region. Label overlap between automatic and manual segmentation (reference) was assessed using the Jaccard index. SD: standard deviation. CV: coefficient of variation (SD/mean, expressed as a percentage). Mean volume error: $100 \times (\text{reference volume} - \text{automatic volume}) / \text{reference volume}$ calculated per individual value pair, then averaged over subjects.

Label	Name	Side	Mean reference volume (mm ³)	Mean automatic volume (mm ³)	Jaccard index	Jaccard SD	Jaccard CV (%)	Mean volume error (n=30) (%)
86	ASG	L	2333	2390	0.68	0.08	12	0.21
87	ASG	R	2233	2281	0.65	0.09	14	0.63
88	MSG	L	1163	1115	0.61	0.12	20	-3.95
89	MSG	R	1193	1038	0.56	0.12	21	-7.01
90	PSG	L	1573	1580	0.67	0.08	12	-0.41
91	PSG	R	1731	1754	0.68	0.07	11	2.18
92	AIC	L	2276	2235	0.64	0.06	10	-3.05
93	AIC	R	2251	2357	0.64	0.08	13	-5.15
94	ALG	L	2642	2635	0.66	0.09	14	-3.82
95	ALG	R	2636	2623	0.68	0.04	5	-9.65
20	PLG	L	2732	2656	0.66	0.06	8	-1.65
21	PLG	R	2883	2794	0.66	0.06	9	-0.002

4.1. Subdivisions

We defined protocols for dividing the insula into six subregions and applied them to 30 right and 30 left hemispheres. Our work also enabled us to create the first probabilistic maps of insular subdivisions according to macroanatomical landmarks. Important strengths of these maps are that they pertain to MNI152 space and are thus usable through standard software packages, and that they account for inter-individual variability by virtue of being built from multiple atlases. This will help anatomical localization especially. Even without knowledge of underlying cytoarchitectonical subdivisions, it can be observed that insular gyri differ in their electrophysiological responses (e.g. Frot et al., 2014), as well as in their BOLD activations (e.g. Mazzola et al., 2012; Pomares et al., 2013) to the same stimulus. In addition, multiple structural and functional MR contrasts have allowed deterministic division of the whole insula by semi-automatic *in vivo* methods using surface-based analysis (Glasser et al., 2016). The overall shape of the insular subdivisions thus derived closely matches macroanatomy (compare Fig. 14 in Supplementary Material 3 from Glasser et al. (2016) with our Fig. 3 and graphical abstract). Our maps are complementary in that they have been volumetrically derived and thus can be used for localization during standard volumetric brain-mapping studies, and also in that they incorporate probabilistic localisation information.

Our maps are complementary to the cytoarchitectonically defined probabilistic maps made by Kurth et al. (2010) on 10 brains reported in MNI152 space. However, their maps cover only a part of the posterior insula. The architectonic and macroanatomical organization of the insula differ: for example, cytoarchitectonic gradients may run nearly orthogonal to the orientation of the sulci, an observation also made in non-human primates (Evrard et al., 2014; Morel et al., 2013; Nieuwenhuys, 2012). While the macroanatomical boundary of the insula is the peri-insular sulcus, this is not true for the cytoarchitectonical boundaries. For example, the superior part of the ALG as defined in our work is classified as SII opercular cortex (OP3 or OP2) according to cytoarchitectonic maps (Eickhoff et al., 2006). In the same vein, the *dorsal posterior insular region* defined by Craig (2002) according to functional results, is actually not completely included in the insula. Instead, it is located in the PIS, which is classified as operculum in most atlases and spreads partly into the superior part of ALG, like the region OP2 defined by Eickhoff et al. (2006) does. Joint cytoarchitectonic / macroanatomical maps could be important tools to enable accurate anatomical localization and to prevent confusion.

Cortical function has long been known to be associated with sulcal patterns (Welker and Johnson, 1965). On several occasions, only advanced knowledge of sulcal patterns has allowed linking a specific function to a specific sulcal configuration. Prominent examples are 1) the human area V5 (Watson et al., 1993), 2) posterior frontolateral

activations observed in task-switching (consistently and reliably located at the junction of the inferior frontal sulcus and the inferior precentral sulcus (Derrfuss et al., 2009)) and 3) the hand area always being linked to the cingulate sulcus, even when a paracingulate gyrus is present (Amiez and Petrides, 2014). While *prima facie* no such correlations exist in the insula, a thorough definition of insular anatomy including its statistical variation is a prerequisite to detecting any such relationships, should they exist.

The insula is increasingly recognized as a seat of epileptogenic foci (Isnard et al., 2004, 2000; Picard and Kurth, 2014; Ryvlin et al., 2006). Better means of accurately describing the localization of e.g. PET or ictal SPECT/SISCOM abnormalities are needed. In these situations, cytoarchitectonic maps are dispensable, but macroanatomical landmarks bridge imaging, neurosurgical navigation software, and direct visualization during neurosurgery. They are also useful for placement of depth electrodes for stereo-EEG, as the insular gyri differ in electrophysiological characteristics (Frot et al., 2014).

4.2. Morphology

Our findings of global insula morphology are in accordance with previous descriptions (Affif et al., 2013; Naidich et al., 2004; Nieuwenhuys, 2012; Rosen et al., 2015; Türe et al., 1999). The CS is a highly consistent feature across subjects. Of the five main gyri, the MSG is the smallest and shows high variability in terms of size and location. The only discordant point between our study and some of the previous literature is the prevalence of the accessory and transverse gyri. Presence of an AG has previously been described in more than 82% of insulae, and a TG in more than 86% on the anterior face of the insula (Affif et al., 2013; Naidich et al., 2004; Nieuwenhuys, 2012; Türe et al., 1999). In our data, we noticed their presence in only 57% for TG and 50% for AG, similar to Rosen et al. (2015), where AG was absent in 37% of cases. This difference probably arises from the way these gyri are identified. We defined AG as a separate gyrus from ASG only when there was a sulcus (e.g. Fig. 3: A5LR & A8R & A29R). Also, TG was separated from the pole when a sulcus was identified between these structures. However, inspecting the anterior face of the insula on 3D projections, there was often a boundary between the inferior and superior part: a sulcus (TS) in 57% of insulae, or at least a curvature where the orbital cortex bends into the insula. This can be seen as two oblique gyri extending to the lateral surface, as a junction between the frontoorbital region and the lateral insula. Fig. 6 shows an insula where we did not distinguish the ASG from AG, but one can easily imagine two oblique gyri when looking at the anterior surface (see right panel of Fig. 6C). Türe et al. (1999) included both gyri in the pole but, as there was often no boundary between ASG and AG (e.g. A03L Figs. 3 and 6), we preferred to include the AG in the ASG region. Rosen et al. (2015) did not define TG in their insular topology rendering and did not

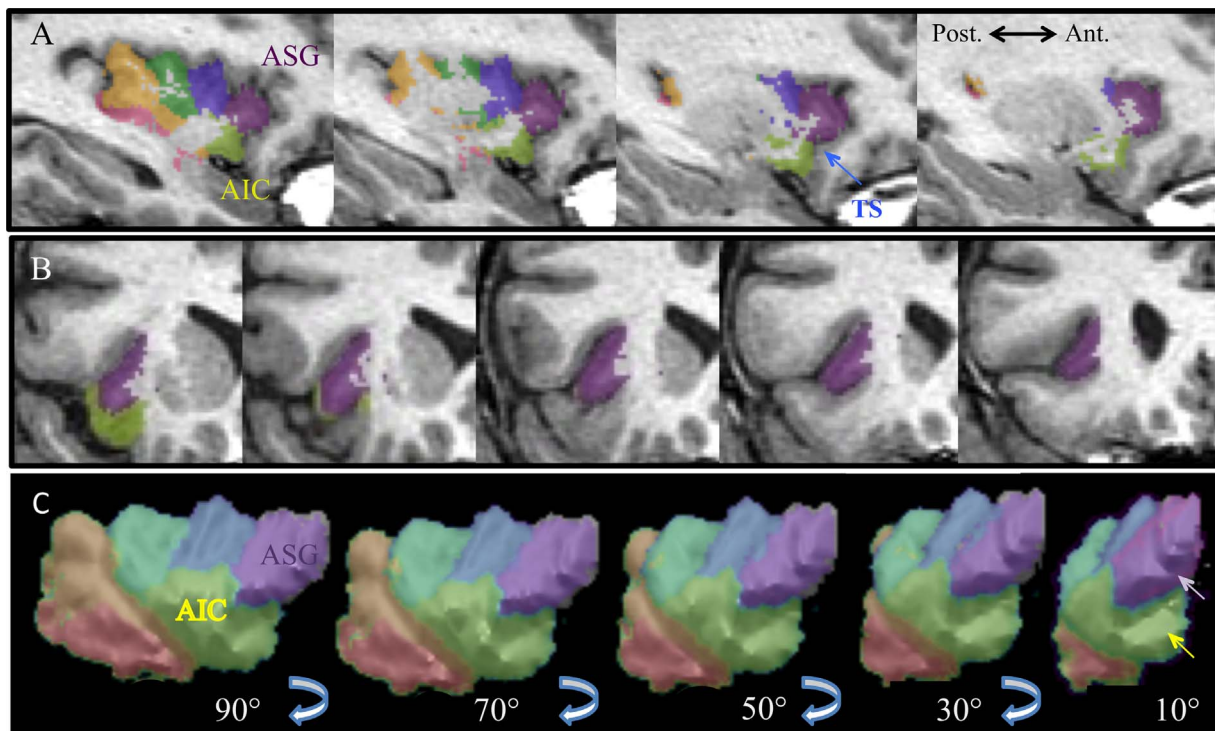


Fig. 6. Example of an image where there could be a discordant identification of anterior gyri. Sagittal (A) and coronal (B) slices of the left insula of subject 3 (every 3 mm). C. 3D-rendering of this insula viewing the lateral surface (viewing angles from 90° to 10°, i.e. from a strictly lateral view to a nearly completely anterior view). There is no accessory gyrus (AG) based on our definition, since there is only one gyrus visible on the sagittal slices (A). However, as the anterior short gyrus (ASG purple) and the anterior inferior cortex (AIC yellow) extend medially, the anterior surface shows two gyri (arrows at 10°), named AG and transverse gyrus (TG) by Türe et al. (1999) and Naidich et al. (2004).

provide a clear description of AG. The structure labelled AG in their figure might be TG, or alternatively an additional anterior gyrus. Moreover, they noticed that the dorsal border of their AG did not extend as far as the adjacent ASG, which could correspond to our TG description. Finally, the anterior face of the insula shows variability with occurrence of “bumps” that can be seen as additional gyri (AG, TG) or as a bifid ASG or extension of the pole.

The PLG, as defined by our protocol, is very stable in its volume and its localization in MNI152 space because its inferior limit is the PIS, which is a stable and preeminent sulcus. However, the gyrus itself is often flat and its superior border is artificial (between the ends of the PostCS and the CS). This is why the strategy of Rosen et al. (2015) has difficulty to dissociate this gyrus. Afff et al. (2013) also noted that the PLG is the most constant gyrus of the insula. This could be explained by the early fetal development of the posterior part of the Sylvian fissure (Afff et al., 2009).

The relation between the insular gyri and the opercula is congruent with the observations of Türe et al. (1999), except for the PLG. In our study, in more than 90% of cases, ASG and MSG were covered by the IFG; PSG was covered by the PreCG; and ALG was covered by the PostCG. We never found the PLG to be in contact with the parietal operculum. Instead, it was always under the temporal operculum. Roughly speaking, we found that the anterior insula is covered by frontal cortex and the posterior insula is covered by parietal cortex, as also stated by Naidich et al. (2004).

4.3. Volumes

The mean volume of the insular GM in individual space was $7.7 \pm 0.9 \text{ cm}^3$, corroborating the results previously obtained using automated segmentation: $7.6 \pm 0.9 \text{ cm}^3$ for healthy males (Koenders et al., 2015) and $6.6 \pm 0.5 \text{ cm}^3$ (Durazzo et al., 2011); or after manual segmentation: $8.7 \pm 0.9 \text{ cm}^3$ (Semendeferi and Damasio, 2000); or estimated after histological processing: $6.3 \pm 1.4 \text{ cm}^3$ (Bauernfeind et al., 2013);

but contrasting with the $4.6 \pm 0.8 \text{ cm}^3$ found by Afff et al. (2013).

Afff et al. (2013) noted that the absolute insula volumes were smaller in women than in men, as replicated in our data. However, we showed that when insular volumes are expressed relative to the volume of the ipsilateral GM or of the whole brain (ICV), the insula in women represented a slightly larger portion of the brain than in men, an observation that has not been described before.

We did not find any side or age effect. The lack of an age effect is not surprising, considering that it was also found by Hammers et al. (2003) on 20 of the same images, albeit with volumes that included white matter. In any case, age effects would be difficult to detect on this homogeneous sample (healthy controls aged 20–54). Good et al. (2001) found little positional asymmetry of the insula in a voxel-based morphometry study (not measuring absolute volumes) and found no influence of handedness anywhere in the brain when comparing 67 left-handers with 398 right-handers. As hemispheric language dominance was not assessed in our sample, we could not replicate a finding of a positive correlation between the extent of hemispheric language dominance and insula volume asymmetry (Keller et al. 2010).

4.4. Future uses

In previous work, we have shown that high-quality individual atlases can be used in a multi-atlas propagation and label fusion framework to provide automatic segmentations that are comparable in accuracy to manual delineations (Hammers et al., 2007a; Heckemann et al., 2006). Such strategies have been extended to enable automatic segmentation of the brains of children as young as two years (Gousias et al., 2008), one year (Gousias et al., 2012), and neonates (Gousias et al., 2013), as well as older subjects (e.g. > 80 years of age) and patients with neurodegenerative disease (Heckemann et al., 2011, 2010). Our leave-one-out MAPER experiment verifies that the new insula subregions can be reproduced with the expected high level of accuracy. Describing any possible structure-function relationships

naturally requires structure to be suitably defined; our atlas material in conjunction with multi-atlas label propagation will enable exactly this. In the past, this approach has yielded results that are the basis for our optimism (see e.g. Sapey-Triomphe et al., 2015).

Such strategies should facilitate and extend functional or connectivity studies, which in the past have relied on fixed-sized ROIs to sample parts of insular gyri (Cauda et al., 2011), or have used voxel-based measures within a whole insula ROI defined individually (Cerliani et al., 2012), or defined once for all participants on an average MRI (Deen et al., 2011). Conceivably, taking into account the high interindividual consistency of cytoarchitectonic areas at least in the posterior insula (Kurth et al., 2010a), as well as areas detected through multimodal *in vivo* segmentation (Glasser et al., 2016), any existing function-sulcus relationships might become detectable through the use of subject-specific segmentations. The cytoarchitectonic study of brains with *ex vivo* MRI could equally help to study any such relationship, as could the study of insular hodology and the comparison with non-human primates. Notwithstanding these perspectives, as they stand, our maps provide only complementary information to parcellations based on cytoarchitecture, function, or hodology; they do not show direct associations or relationships.

It is interesting that when Brodmann described the antero-posterior organization in a clearly different posterior granular and an anterior agranular cortex, he also stated that the boundary was along the central sulcus of the insula, albeit not exactly (“nicht genau”, Brodmann, 1909, p. 146 and Fig. 89 p. 144). This antero-posterior organization remains consistent with more recent studies (e.g. Kurth et al., 2010a, Glasser et al. 2016). The insula seems to be an exception to the idea that major sulci are good average indicators of cytoarchitecture and, by inference, functional regions (cf. Hammers et al., 2007a). However, an anatomical atlas can help to accurately localize cytoarchitectonic areas since their macro-anatomical locations are quite stable across subjects when considering a Cartesian coordinate system of a 3D brain volume (Kurth et al. 2010a). If there is correspondence between functional and cytoarchitectonic areas, as findings of very localized activations e.g. to thermosensory stimuli (Craig et al. 2000) suggest, then these should correspond to localized *average* across-subject correspondences of cytoarchitectonics in stereotaxic space (cf. Kurth et al. 2010a). Our results will aid in ascribing such group findings to gyral locations.

The thoroughly tested protocols created as part of this work have proved to be applicable to a large number of hemispheres (n=60) and will facilitate manual delineations by other scientists as well.

5. Conclusion

The creation of dependable protocols and manual delineation of sixty human insulae enabled the construction of probabilistic and stereotactic maps of six subdivisions according to macroanatomical landmarks: four anterior regions (three short gyri and the anterior inferior cortex) and two posterior long gyri. After spatial normalization, probabilistic atlases have been created and new individual atlases and a new maximum probability map (Hammers_mith n30r95) integrating the newly added angular and supramarginal gyri (Wild et al., submitted), are freely downloadable for academic use from <http://www.brain-development.org> (for referees: available at <http://soundray.org/hammers-n30r95>). The equally available individual atlases will enable individual MRIs to be segmented into insular subregions via multi-atlas techniques like MAPER, with good accuracy as quantified in this paper.

Acknowledgements

We would like to thank Colin Studholme for providing the RView software and support, Heather Wild for coordinating her parallel work on parietal lobe division, and Afif Afif for reviewing the original protocol.

The Hammers_mith atlases are available via free academic licences at <http://www.brain-development.org>. The papers documenting the creation of the original atlases up to 83 regions (© Copyright Imperial College of Science, Technology and Medicine 2007. All rights reserved) are Hammers A, Allom R et al., Hum Brain Mapp 2003 for regions 1–49 and the principle; Gousias IS et al. Neuroimage 2008 for regions 50–83.

Appendix A. Supplementary material

Supplementary data associated with this article can be found in the online version at doi:10.1016/j.neuroimage.2017.01.073.

References

- Aff, A., Becq, G., Mertens, P., 2013. Definition of a stereotactic 3-dimensional magnetic resonance imaging template of the human insula. *Neurosurgery* 72, 35–46. <http://dx.doi.org/10.1227/NEU.0b013e31826cdc57>.
- Aff, A., Hoffmann, D., Becq, G., Guenot, M., Magnin, M., Mertens, P., 2009. MRI-based definition of a stereotactic two-dimensional template of the human insula. *Stereotact. Funct. Neurosurg.* 87, 385–394. <http://dx.doi.org/10.1159/000258079>.
- Amiez, C., Petrides, M., 2014. Neuroimaging evidence of the anatomo-functional organization of the human cingulate motor areas. *Cereb. Cortex N. Y. N* 1991 (24), 563–578. <http://dx.doi.org/10.1093/cercor/bhs329>.
- Ashburner, J., Friston, K.J., 2005. Unified segmentation. *NeuroImage* 26, 839–851. <http://dx.doi.org/10.1016/j.neuroimage.2005.02.018>.
- Bauernfeind, A.L., de Sousa, A.A., Avasthi, T., Dobson, S.D., Raghanti, M.A., Lewandowski, A.H., Zilles, K., Semendeferi, K., Allman, J.M., (Bud) Craig, A.D., Hof, P.R., Sherwood, C.C., 2013. A volumetric comparison of the insular cortex and its subregions in primates. *J. Hum. Evol.* 64, 263–279. <http://dx.doi.org/10.1016/j.jhevol.2012.12.003>.
- Bonthuis, D.J., Solodkin, A., Van Hoesen, G.W., 2005. Pathology of the insular cortex in Alzheimer disease depends on cortical architecture. *J. Neuropathol. Exp. Neurol.* 64, 910–922.
- Brockhaus, H., 1940. Die Cyto- und Myeloarchitektonik des Cortex claustralis und des Claustrum beim Menschen. *J. Psychol. Neurol.* 49, 249–348.
- Brodmann, K., 1909. Vergleichende Lokalisationslehre der Grosshirnrinde in ihren Prinzipien dargestellt und Grund des Zellenbaues. J.A. Barth., Leipzig.
- Cauda, F., D'Agata, F., Sacco, K., Duca, S., Geminiani, G., Vercelli, A., 2011. Functional connectivity of the insula in the resting brain. *NeuroImage* 55, 8–23. <http://dx.doi.org/10.1016/j.neuroimage.2010.11.049>.
- Cerliani, L., Thomas, R.M., Jbabdi, S., Siero, J.C.W., Nanetti, L., Crippa, A., Gazzola, V., D'Arceuil, H., Keysers, C., 2012. Probabilistic tractography recovers a rostrocaudal trajectory of connectivity variability in the human insular cortex. *Hum. Brain Mapp.* 33, 2005–2034. <http://dx.doi.org/10.1002/hbm.21338>.
- Craig, A.D., 2002. How do you feel? Interoception: the sense of the physiological condition of the body. *Nat. Rev. Neurosci.* 3, 655–666. <http://dx.doi.org/10.1038/nrn894>.
- Craig, A.D.B., 2009. How do you feel — now? The anterior insula and human awareness. *Nat. Rev. Neurosci.* 10, 59–70. <http://dx.doi.org/10.1038/nrn2555>.
- Craig, A.D., Chen, K., Bandy, D., Reiman, E.M., 2000. Thermosensory activation of insular cortex. *Nat. Neurosci.* 3, 184–190. <http://dx.doi.org/10.1038/72131>.
- Cunningham, D., 1891. The development of the gyri and sulci on the surface of the island of Reil of the human brain. *J. Anat. Physiol.*, 338–348.
- Deen, B., Pitskel, N.B., Pelphrey, K.A., 2011. Three systems of insular functional connectivity identified with cluster analysis. *Cereb. Cortex N. Y. N* 1991 (21), 1498–1506. <http://dx.doi.org/10.1093/cercor/bhq186>.
- Derrfuss, J., Brass, M., von Cramon, D.Y., Lohmann, G., Amunts, K., 2009. Neural activations at the junction of the inferior frontal sulcus and the inferior precentral sulcus: interindividual variability, reliability, and association with sulcal morphology. *Hum. Brain Mapp.* 30, 299–311. <http://dx.doi.org/10.1002/hbm.20501>.
- Durazzo, T.C., Tosun, D., Buckley, S., Gazdzinski, S., Mon, A., Fryer, S.L., Meyerhoff, D.J., 2011. Cortical thickness, surface area and volume of the brain reward system in alcohol dependence: relationships to relapse and extended abstinence. *Alcohol. Clin. Exp. Res* 35, 1187–1200. <http://dx.doi.org/10.1111/j.1530-0277.2011.01452.x>.
- Eickhoff, S.B., Schleicher, A., Zilles, K., Amunts, K., 2006. The human parietal operculum. I. Cytoarchitectonic mapping of subdivisions. *Cereb. Cortex N. Y. N* 1991 (16), 254–267. <http://dx.doi.org/10.1093/cercor/bhi105>.
- Eickhoff, S.B., Stephan, K.E., Mohlberg, H., Grefkes, C., Fink, G.R., Amunts, K., Zilles, K., 2005. A new SPM toolbox for combining probabilistic cytoarchitectonic maps and functional imaging data. *NeuroImage* 25, 1325–1335. <http://dx.doi.org/10.1016/j.neuroimage.2004.12.034>.
- Evraud, H.C., Logothetis, N.K., (Bud) Craig, A. d., 2014. Modular architectonic organization of the insula in the macaque monkey. *J. Comp. Neurol.* 522, 64–97. <http://dx.doi.org/10.1002/cne.23436>.
- Frot, M., Faillenot, I., Mauguère, F., 2014. Processing of nociceptive input from posterior to anterior insula in humans. *Hum. Brain Mapp.* <http://dx.doi.org/10.1002/hbm.22565>.
- Garcia-Larrea, L., 2012. The posterior insular-opercular region and the search of a primary cortex for pain. *Neurophysiol. Clin. Clin. Neurophysiol.* 42, 299–313.

- <http://dx.doi.org/10.1016/j.neucli.2012.06.001>.
- Glasser, M.F., Coalson, T.S., Robinson, E.C., Hacker, C.D., Harwell, J., Yacoub, E., Ugurbil, K., Andersson, J., Beckmann, C.F., Jenkinson, M., Smith, S.M., Van Essen, D.C., 2016. A multi-modal parcellation of human cerebral cortex. *Nature* 536, 171–178.
- Good, C.D., Johnsrude, I., Ashburner, J., Henson, R.N., Friston, K.J., Frackowiak, R.S., 2001. Cerebral asymmetry and the effects of sex and handedness on brain structure: a voxel-based morphometric analysis of 465 normal adult human brains. *NeuroImage* 14, 685–700. <http://dx.doi.org/10.1006/nimg.2001.0857>.
- Gousias, I.S., Hammers, A., Counsell, S.J., Edwards, A.D., Rueckert, D., 2012. Automatic segmentation of pediatric brain MRIs using a maximum probability pediatric atlas. In: *Proceedings of the 2012 IEEE International Conference on Imaging Systems and Techniques (IST)*. Presented at the 2012 IEEE International Conference on Imaging Systems and Techniques (IST), pp. 95–100. <http://dx.doi.org/10.1109/IST.2012.6295511>.
- Gousias, I.S., Hammers, A., Counsell, S.J., Srinivasan, L., Rutherford, M.A., Heckemann, R.A., Hajnal, J.V., Rueckert, D., Edwards, A.D., 2013. Magnetic resonance imaging of the newborn brain: automatic segmentation of brain images into 50 anatomical regions. *PLoS One* 8, e59990. <http://dx.doi.org/10.1371/journal.pone.0059990>.
- Gousias, I.S., Rueckert, D., Heckemann, R.A., Dyet, L.E., Boardman, J.P., Edwards, A.D., Hammers, A., 2008. Automatic segmentation of brain MRIs of 2-year-olds into 83 regions of interest. *NeuroImage* 40, 672–684. <http://dx.doi.org/10.1016/j.neuroimage.2007.11.034>.
- Hammers, A., Allom, R., Koepp, M.J., Free, S.L., Myers, R., Lemieux, L., Mitchell, T.N., Brooks, D.J., Duncan, J.S., 2003. Three-dimensional maximum probability atlas of the human brain, with particular reference to the temporal lobe. *Hum. Brain Mapp.* 19, 224–247. <http://dx.doi.org/10.1002/hbm.10123>.
- Hammers, A., Chen, C.-H., Lemieux, L., Allom, R., Vossos, S., Free, S.L., Myers, R., Brooks, D.J., Duncan, J.S., Koepp, M.J., 2007a. Statistical neuroanatomy of the human inferior frontal gyrus and probabilistic atlas in a standard stereotaxic space. *Hum. Brain Mapp.* 28, 34–48. <http://dx.doi.org/10.1002/hbm.20254>.
- Hammers, A., Heckemann, R., Koepp, M.J., Duncan, J.S., Hajnal, J.V., Rueckert, D., Aljabar, P., 2007b. Automatic detection and quantification of hippocampal atrophy on MRI in temporal lobe epilepsy: a proof-of-principle study. *NeuroImage* 36, 38–47. <http://dx.doi.org/10.1016/j.neuroimage.2007.02.031>.
- Heckemann, R.A., Hajnal, J.V., Aljabar, P., Rueckert, D., Hammers, A., 2006. Automatic anatomical brain MRI segmentation combining label propagation and decision fusion. *NeuroImage* 33, 115–126. <http://dx.doi.org/10.1016/j.neuroimage.2006.05.061>.
- Heckemann, R.A., Keihaninejad, S., Aljabar, P., Gray, K.R., Nielsen, C., Rueckert, D., Hajnal, J.V., Hammers, A., Alzheimer's Disease Neuroimaging Initiative, 2011. Automatic morphometry in Alzheimer's disease and mild cognitive impairment. *NeuroImage* 56, 2024–2037. <http://dx.doi.org/10.1016/j.neuroimage.2011.03.014>.
- Heckemann, R.A., Keihaninejad, S., Aljabar, P., Rueckert, D., Hajnal, J.V., Hammers, A., Alzheimer's Disease Neuroimaging Initiative, 2010. Improving intersubject image registration using tissue-class information benefits robustness and accuracy of multi-atlas based anatomical segmentation. *NeuroImage* 51, 221–227. <http://dx.doi.org/10.1016/j.neuroimage.2010.01.072>.
- Hervé, P.-Y., Crivello, F., Percey, G., Mazoyer, B., Tzourio-Mazoyer, N., 2006. Handedness and cerebral anatomical asymmetries in young adult males. *NeuroImage* 29, 1066–1079. <http://dx.doi.org/10.1016/j.neuroimage.2005.08.031>.
- Ibañez, A., Gleichgerricht, E., Manes, F., 2010. Clinical effects of insular damage in humans. *Brain Struct. Funct.* 214, 397–410. <http://dx.doi.org/10.1007/s00429-010-0256-y>.
- Isnard, J., Guénot, M., Ostrowsky, K., Sindou, M., Mauguère, F., 2000. The role of the insular cortex in temporal lobe epilepsy. *Ann. Neurol.* 48, 614–623.
- Isnard, J., Guénot, M., Sindou, M., Mauguère, F., 2004. Clinical manifestations of insular lobe seizures: a stereo-electroencephalographic study. *Epilepsia* 45, 1079–1090. <http://dx.doi.org/10.1111/j.0013-9580.2004.68903.x>.
- Jaccard, P., 1901. Distribution de la Flore Alpine dans le Bassin des Dranses et dans quelques régions voisines. *Bull. Soc. Vaudoise Sci. Nat.* 37, 241–272.
- Jenkinson, M., Beckmann, C.F., Behrens, T.E.J., Woolrich, M.W., Smith, S.M., 2012. FSL. *NeuroImage* 62, 782–790. <http://dx.doi.org/10.1016/j.neuroimage.2011.09.015>.
- Jones, C.L., Ward, J., Critchley, H.D., 2010. The neuropsychological impact of insular cortex lesions. *J. Neurol. Neurosurg. Psychiatry* 81, 611–618. <http://dx.doi.org/10.1136/jnnp.2009.193672>.
- Keller, S.S., Roberts, N., García-Fiñana, M., Mohammadi, S., Ringelstein, E.B., Knecht, S., Deppe, M., 2010. Can the Language-dominant Hemisphere Be Predicted by Brain Anatomy? *J. Cogn. Neurosci.* 23, 2013–2029. <http://dx.doi.org/10.1162/jocn.2010.21563>.
- Koenders, L., Machielsen, M., van der Meer, F., van Gassel, A., Meijer, C., van den Brink, W., Koeter, M., Caan, M., Cousijn, J., den Braber, A., van 't Ent, D., Rive, M., Schene, A., van de Giessen, E., Huyser, C., de Kwaastniet, B., Veltman, D., de Haan, L., 2015. Brain volume in male patients with recent onset schizophrenia with and without cannabis use disorders. *J. Psychiatry Neurosci.* 40, 197–206. <http://dx.doi.org/10.1503/jpn.140081>.
- Kurth, F., Eickhoff, S.B., Schleicher, A., Hoemke, L., Zilles, K., Amunts, K., 2010a. Cytoarchitecture and probabilistic maps of the human posterior insular cortex. *Cereb. Cortex N. Y. N 1991* (20), 1448–1461. <http://dx.doi.org/10.1093/cercor/bhp208>.
- Kurth, F., Zilles, K., Fox, P.T., Laird, A.R., Eickhoff, S.B., 2010b. A link between the systems: functional differentiation and integration within the human insula revealed by meta-analysis. *Brain Struct. Funct.* 214, 519–534. <http://dx.doi.org/10.1007/s00429-010-0255-z>.
- Lemieux, L., Hammers, A., Mackinnon, T., Liu, R.S.N., 2003. Automatic segmentation of the brain and intracranial cerebrospinal fluid in T1-weighted volume MRI scans of the head, and its application to serial cerebral and intracranial volumetry. *Magn. Reson. Med. J. Soc. Magn. Reson. Med. Soc. Magn. Reson. Med.* 49, 872–884. <http://dx.doi.org/10.1002/mrm.10436>.
- Mazzola, L., Faillenot, I., Barral, F.-G., Mauguère, F., Peyron, R., 2012. Spatial segregation of somato-sensory and pain activations in the human operculo-insular cortex. *NeuroImage* 60, 409–418. <http://dx.doi.org/10.1016/j.neuroimage.2011.12.072>.
- Mesulam, M., Mufson, E., 1985. The Insula of Reil in Man and Monkey. *Architectonics, Connectivity, and Function*. In: *Cerebral Cortex*, Plenum Publishing Corporation, Peters A, Jones E, 179–224.
- Morel, A., Galloway, M.N., Baechler, A., Wyss, M., Galloway, D.S., 2013. The human insula: architectonic organization and postmortem MRI registration. *Neuroscience* 236, 117–135. <http://dx.doi.org/10.1016/j.neuroscience.2012.12.076>.
- Naidich, T.P., Kang, E., Fatterpekar, G.M., Delman, B.N., Gultekin, S.H., Wolfe, D., Ortiz, O., Yousry, I., Weismann, M., Yousry, T.A., 2004. The insula: anatomic study and MR imaging display at 1.5 T. *AJNR Am. J. Neuroradiol.* 25, 222–232.
- Nieuwenhuis, R., 2012. The insular cortex: a review. *Prog. Brain Res.* 195, 123–163. <http://dx.doi.org/10.1016/B978-0-444-53860-4.00007-6>.
- Ostrowsky, K., Magnin, M., Rylvlin, P., Isnard, J., Guénot, M., Mauguère, F., 2002. Representation of pain and somatic sensation in the human insula: a study of responses to direct electrical cortical stimulation. *Cereb. Cortex N. Y. N 1991* (12), 376–385.
- Peyron, R., Schneider, F., Faillenot, I., Convers, P., Barral, F.-G., Garcia-Larrea, L., Laurent, B., 2004. An fMRI study of cortical representation of mechanical allodynia in patients with neuropathic pain. *Neurology* 63, 1838–1846.
- Picard, F., Kurth, F., 2014. Ictal alterations of consciousness during ecstatic seizures. *Epilepsy Behav.* EB 30, 58–61.
- Pomares, F.B., Faillenot, I., Barral, F.G., Peyron, R., 2013. The “where” and the “when” of the BOLD response to pain in the insular cortex. Discussion on amplitudes and latencies. *NeuroImage* 64, 466–475. <http://dx.doi.org/10.1016/j.neuroimage.2012.09.038>.
- Rose, M., 1928. Die Inselrinde des Menschen und der Tiere. *J. Fuer Psychol. Neurol.* 467–624.
- Rosen, A., Chen, D.Q., Hayes, D.J., Davis, K.D., Hodaie, M., 2015. A Neuroimaging Strategy for the Three-Dimensional in vivo Anatomical Visualization and Characterization of Insular Gyri. *Stereotact. Funct. Neurosurg.* 93, 255–264. <http://dx.doi.org/10.1159/000380826>.
- Rylvlin, P., Minotti, L., Demarquay, G., Hirsch, E., Arzimanoglou, A., Hoffman, D., Guénot, M., Picard, F., Rheims, S., Kahane, P., 2006. Nocturnal hypermotor seizures, suggesting frontal lobe epilepsy, can originate in the insula. *Epilepsia* 47, 755–765. <http://dx.doi.org/10.1111/j.1528-1167.2006.00510.x>.
- Sapey-Triomphe, L.-A., Heckemann, R.A., Boublay, N., Dorey, J.-M., Hénaff, M.-A., Rouch, I., Padovan, C., Hammers, A., Krolak-Salmon, P., Alzheimer's Disease Neuroimaging Initiative, 2015. Neuroanatomical correlates of recognizing face expressions in mild stages of Alzheimer's Disease. *PLoS One* 10, e0143586. <http://dx.doi.org/10.1371/journal.pone.0143586>.
- Semendeferi, K., Damasio, H., 2000. The brain and its main anatomical subdivisions in living hominoids using magnetic resonance imaging. *J. Hum. Evol.* 38, 317–332. <http://dx.doi.org/10.1006/jhev.1999.0381>.
- Tramo, M.J., Loftus, W.C., Thomas, C.E., Green, R.L., Mott, L.A., Gazzaniga, M.S., 1995. Surface area of human cerebral cortex and its gross morphological subdivisions: in vivo measurements in monozygotic twins suggest differential hemisphere effects of genetic factors. *J. Cogn. Neurosci.* 7, 292–302. <http://dx.doi.org/10.1162/jocn.1995.7.2.292>.
- Türe, U., Yaşargil, D.C., Al-Mefty, O., Yaşargil, M.G., 1999. Topographic anatomy of the insular region. *J. Neurosurg.* 90, 720–733.
- Watson, J.D., Myers, R., Frackowiak, R.S., Hajnal, J.V., Woods, R.P., Mazziotta, J.C., Shipp, S., Zeki, S., 1993. Area V5 of the human brain: evidence from a combined study using positron emission tomography and magnetic resonance imaging. *Cereb. Cortex N. Y. N 1991* (3), 79–94.
- Welker, W.I., Johnson, J.L., 1965. Correlation between nuclear morphology and somatotopic organization in ventro-basal complex of the raccoon's thalamus. *J. Anat.* 99, 761–790.